ORIGINAL ARTICLE

A direct ROI quantification method for inherent PVE correction: accuracy assessment in striatal SPECT measurements

**Eleonora Vanzi · Maria Teresa De Cristofaro ·
Silvia Ramat · Barbara Sotgia · Mario Mascalchi ·
Andreas Robert Formiconi**

Abstract

Purpose The clinical potential of striatal imaging with dopamine transporter (DAT) SPECT tracers is hampered by the limited capability to recover activity concentration ratios due to partial volume effects (PVE). We evaluated the accuracy of a least squares method that allows retrieval of activity in regions of interest directly from projections (LS-ROI).

Methods An Alderson striatal phantom was filled with striatal to background ratios of 6:1, 9:1 and 28:1; the striatal and background ROIs were drawn on a coregistered X-ray CT of the phantom. The activity ratios of these ROIs were derived both with the LS-ROI method and with conventional SPECT EM reconstruction (EM-SPECT). Moreover, the two methods were compared in seven patients with motor symptoms who were examined with *N*-3-fluoropropyl-2-β-carboxymethoxy-3-β-(4-iodophenyl) (FP-CIT) SPECT, calculating the binding potential (BP).

Results In the phantom study, the activity ratios obtained with EM-SPECT were 3.5, 5.3 and 17.0, respectively, whereas the LS-ROI method resulted in ratios of 6.2, 9.0 and 27.3, respectively. With the LS-ROI method, the BP in the seven patients was approximately 60% higher than with EM-SPECT; a linear correlation between the LS-ROI and the EM estimates was found ($r=0.98$, $p=0.03$).

Conclusion The LS-ROI PVE correction capability is mainly due to the fact that the ill-conditioning of the LS-ROI approach is lower than that of the EM-SPECT one. The LS-ROI seems to be feasible and accurate in the examination of the dopaminergic system. This approach can be fruitful in monitoring of disease progression and in clinical trials of dopaminergic drugs.

Introduction

Imaging of dopamine transporters using single-photon emission computed tomography (SPECT) has been introduced as a valuable tool to evaluate patients with Parkinson's disease (PD) [1–3]. Even if visual assessment of the images can be considered sufficient in many diagnostic situations [4], a quantitative approach is extremely important in novel promising perspectives, such as the measurement of disease progression and the monitoring of neuroprotective treatments. Quantitative analysis is based on calculation of the binding potential (BP) resulting from the ratio of specific (striatum, caudate, putamen) to non-specific (occipital lobe or cerebellum) activity at steady state.

Accuracy of region of interest (ROI) activity estimation is hampered by attenuation and scatter effects and by the poor spatial resolution of nuclear imaging techniques. The importance of attenuation and scatter corrections in improving the accuracy of quantitative BP measurements has already been pointed out [5, 6]. However, even with these corrections, accurate estimates of activity in ROIs that are often small with respect to the spatial resolution of the tomographic systems are particularly challenging. Indeed,

E. Vanzi (✉) · M. T. De Cristofaro · B. Sotgia · M. Mascalchi · A. R. Formiconi
Clinical Pathophysiology, University of Florence,
Viale Morgagni, 85,
Florence 50134, Italy
e-mail: e.vanzi@dfc.unifi.it

S. Ramat
Neurological and Psychiatric Sciences, University of Florence,
Viale Morgagni, 85,
Florence 50134, Italy

activity is systematically underestimated for objects smaller than 2.5 times the full-width at half-maximum (FWHM) of the point spread function (PSF) [7–9] when their activity is higher than that in the surrounding regions. Conversely, low-activity objects are overestimated owing to the effect of spill-in from high-activity adjacent regions. The loss of signal due to the limited spatial resolution is called the "partial volume effect" (PVE) and the factor that expresses this loss of quantification is called the "recovery coefficient". These considerations are relevant to BP estimates with SPECT, in which radioactivity concentration in the striata can be underestimated by more than 50% if no correction for PVE is applied [5, 10]. In spite of its high spatial resolution and sensitivity, PET is also markedly affected by the PVE [11, 12], and an underestimate of around 50% of the true activity can still be expected when BP measurements are done [13].

In recent years, physical [14–16] or simulated [17] phantom studies have frequently been used to characterise the PVE. Nowadays, the availability of high-resolution structural imaging (X-ray CT or MRI) facilitates the implementation of sophisticated PVE correction procedures [18–20], and several publications have addressed this issue [21–24]. Anyway, all these techniques require some non-trivial procedures for the determination of corrections which are applied, a posteriori, to the ROI activity obtained by summing the values of the individual reconstructed pixels in the volume of interest.

A method with an inherent capability of PVE correction (LS-ROI, see below for the acronym) for the estimation of region activity directly from projections was previously developed by our group [25]. This method does not require an image reconstruction step and allows unbiased regional concentration estimates to be obtained. Its application in dynamic SPECT has previously been evaluated in a study simulating kidney dynamics of radiohippuran [26].

In the present study we applied the LS-ROI method to prevent PVE and to obtain reliable quantitative estimates of the BP in ^{123}I-FP-CIT brain studies. LS-ROI results were compared with the values obtained when activity concentrations were estimated by overlapping ROIs over conventionally reconstructed images without PVE correction. Phantom studies were performed in order to compare the two methods. Results obtained in seven FP-CIT (DATS-CAN, GE Healthcare, Amersham, UK) patient studies are also presented.

Materials and methods

LS-ROI method

The LS-ROI method [25] falls among the "natural" or "generalised" voxel techniques. This class of algorithms is derived from the early work of Huesman [27], extended later to include not only scatter but also spatial resolution effects, both in the heart [28] and in tumour imaging [29]. An alternative formulation assuming Poisson statistics was suggested by Carson [30] and, more recently, a technique called "template projection-reconstruction" [31] was used successfully to quantify target regions in tomographic images.

In such approaches, the object is supposed to be constituted of a few homogeneous ROIs of arbitrary shape. These ROIs are called "natural voxels", since their homogeneous concentration is "naturally" induced by organ structure or tracer distribution. After their delineation, these natural voxels constitute the basic image volume element and the tomographic problem reduces to the determination of their value, just as if they were the standard cubic voxels. Owing to the reduced number of unknowns, the solution can be computed numerically from raw projection data by the direct inversion of the tomographic matrix. In the specific case of the LS-ROI method, the direct solution is evaluated in a least squares sense, hence the name of the method that we propose. The mathematical details of the LS-ROI method are reported in the Appendix. The main feature of quantification with LS-ROI is that conventional image reconstruction is not needed, except for the purely geometrical step of ROI contour drawing, when structural coregistered images are not available.

The hypothesis of region homogeneity required by the method sometimes may be a quite raw approximation of reality. Therefore, its validity has to be assessed every time, and the accuracy of ROI activity estimation increases if this hypothesis is well satisfied. In order to satisfy the homogeneity requirement, ROIs may be subdivided, but increasing the number of ROIs will lead to worsening of noise propagation and ill-conditioning. Thus, a trade-off always has to be made between accuracy and precision of estimates. However, in some kinds of study (such as those with FP-CIT), the tracer really distributes in a few regions, inside any of which the concentration is quite homogeneous. Thus, the application of these methods in dopamine receptor studies seems to be adequate.

System PSF model

In both EM-SPECT and LS-ROI algorithms the depth-dependent system response model described in [32] has been introduced through tomographic coefficients. The increase in the FWHM with the distance between the source and the collimator is modelled in the transaxial planes, while the longitudinal spread is assumed to be that of a voxel in the centre of the reconstruction volume and constant for each source position [33]. The intrinsic camera resolution has also been added to the collimator resolution in order to obtain the total system resolution.
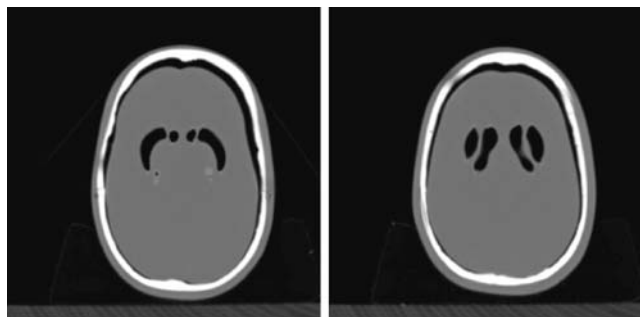
Fig. 1 CT transaxial views of the Alderson phantom through the striata

Phantom study

In order to evaluate the quantitative capabilities of the two methods, we performed two Alderson striatal phantom (Radiological Support Devices Inc., Long Beach, CA, USA) acquisitions. The phantom consists of five anthropomorphic compartments, corresponding to left and right caudate nuclei, left and right putamen, and the remaining brain volume. The compartments are separated by thin polyurethane walls. The chambers are surrounded by an artificial skull that includes both the soft tissue substitute (polyurethane, modified for tissue equivalence) and the skull.

A high-resolution CT image of the phantom was acquired with the brain shell cavity filled with water and the four striatal compartments left empty. Two cross-sectional views of the phantom through the striata are shown in Fig. 1. In the CT scan, 73 slices of 512×512 pixels were acquired (pixel size=0.49 mm, slice thickness=2 mm).

The SPECT acquisitions were performed with a triple-headed camera (IRIX with UHR collimators). Projections were acquired in a matrix of 128×128 bins, bin size= 2.33 mm. The radius of rotation was 15 cm. In both scans, 120 angles were acquired at 120 s each, for a total acquisition time of 80 min.

In the first experiment (Acq 1), the four striatal compartments were filled with the same solution of ^{123}I-iodide. In the remaining part of the brain shell, a more diluted solution was used. Concentrations were measured in a well counter. A 6.11:1 striatum-to-background ratio was measured. In the second experiment (Acq 2), the left and right striatal compartments were filled with two different solutions of ^{99m}Tc. The striata-to-background ratios measured in a well counter were 9.15:1 and 27.87:1 for the right and the left striatum, respectively. Total counts were approximately 2.5 and 1.75 million in the first and the second experiment, respectively.

In order to register the CT and the SPECT images, the tomographic data sets underwent a first EM reconstruction. The CT images were processed in order to manually remove the skull external contribution that is not visible on the SPECT images. Then, the CT images were realigned to the SPECT ones by using the NEUROSTAT software [34]. After the CT images had been coregistered to the SPECT ones, the attenuation map, consisting of the skull and the inner brain compartment, was used for the final EM reconstruction (120 iterations) and for the calculation of the ROIs' sinograms. A homogeneous μ=0.20 cm^{-1} attenuation coefficient was used for Chang attenuation correction.

Region segmentation was performed on the realigned CT images with the MRIcro [35] region segmentation tool. The volumes of the segmented striata and of the remaining brain shell were 8.4 and 1,320 ml, respectively. Background concentration was evaluated with a cylindrical ROI with an elliptical section of 247 voxels extending over ten slices in which striata were also present and it was kept sufficiently far from them to avoid spillover effects. The volume of this reference region was 31.4 ml.

Patient studies

The DATSCAN studies of seven patients were analysed with both methods. A summary of patient symptoms and diagnosis is shown in Table 1. Criteria for possible diagnosis of PD are the presence of at least two of the following features: resting tremor, bradykinesia, rigidity, asymmetrical onset (at least one of these must be tremor or bradykinesia); criteria for probable diagnosis of PD are the presence of at least three of the above-mentioned features [36]. None of the patients was taking interfering drugs.

The SPECT scan was acquired 3 h post injection to obtain a conventional BP estimate [2]: FP-CIT injected dose was 185 MBq and 120 projection angles were

Table 1 Age, diagnosis and symptoms of the seven analysed patients

Pat. no.	Age and sex	Diagnosis	Symptoms
1	53 M	Possible PD	Bradykinesia, asymmetrical onset
2	64 M	Tremor	Postural tremor
3	42 M	Possible PD	Postural tremor, asymmetrical onset
4	74 M	Vascular PD	Diffuse bradykinesia
5	51 F	Parkinsonism	Disequilibrium in familial PD
6	61 M	Probable PD	Rigidity, bradykinesia, asymmetrical onset
7	68 M	Probable PD	Bradykinesia, resting tremor, rigidity

Fig. 2 Ratio estimates on EM images as a function of the iteration number (*iter*) in the phantom studies. Actual striatal/background ratios (*str/bkg*) were: **a** 6.11:1 left and right; **b** 27.87:1 left and 9.15:1 right
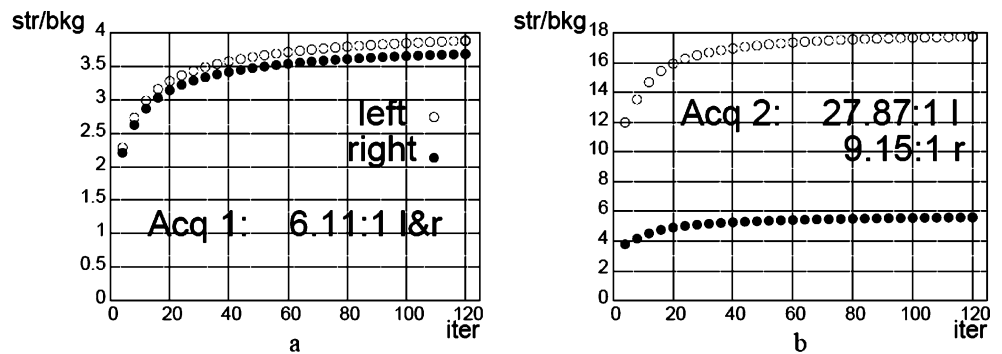
acquired with the same camera and the same projection matrix as in the phantom study. The acquisition time/projection was 60 s. The radius of rotation was settled to the minimum possible value (15.5±1.3 cm). Total counts were, on average, about 2 million.

No scatter correction was applied to the data sets. Chang attenuation correction ($\mu=0.20$ cm^{-1}) was applied. The attenuation mask was evaluated on a four-iteration EM reconstruction by an automated contour detection software based on a thresholding algorithm. Then it was employed both in the final EM reconstruction of the tomographic acquisitions (40 iterations) and in the production of the sinograms.

The ROIs were segmented from the reconstructed 3D image obtained using the EM reconstruction algorithm. The two striatal ROIs were obtained with a thresholding algorithm while cerebellum ROI was obtained by manual segmentation. In order to better satisfy the requirement of region homogeneity needed by the LS-ROI method, the background region was split into two ROIs, one completely void of receptors and the other showing weak binding of the tracer due to the presence of non-specific receptors (like serotonin receptors) that have a certain affinity to DAT. The volumes of striatal and cerebellar ROIs are reported in Table 3.

Results

Phantom study

Conventional ratio estimates obtained by superimposing the ROIs on EM reconstructed images are shown in Fig. 2 as a function of iterations performed. The EM algorithm was used instead of the fastest OSEM version to study the quality and quantification capability of images as "continuously" as possible. A maximum of 120 iterations was performed; however, as shown in Fig. 3, image quality excessively degrades after 40 iterations because of the semiconvergence of iterative algorithms [37]. Therefore, results obtained with 40 iterations will be discussed, since this is a more usual clinical setting. Moreover, ratios obtained after 120 iter-

ations would have produced a reduction of the bias of less than 5% with respect to 40-iteration results.

In Table 2, EM-SPECT ratio values are compared with the LS-ROI estimates. The error in the LS-ROI estimates has been evaluated by propagating the error of the striatal and reference concentrations given by Eq. 10 in the Appendix. On the other hand, estimation of the uncertainty that affects the concentration obtained from reconstructed images is quite a difficult and controversial matter and has not been performed.

Patient studies

Table 3 shows the ratios between activity in striata and cerebellum ($R=(C_{st}-C_{cer})/C_{cer}$) evaluated on patients at 3 h post injection with the EM-SPECT and the LS-ROI method.

A correlation plot between the EM-SPECT and LS-ROI ratio estimates is shown in Fig. 4. The values of R evaluated in the phantom study have also been included in the graph. Linear regression analysis was performed.

Discussion

Phantom study

The importance of SPECT quantification has been increasing since the implementation of molecular imaging techniques like FP-CIT SPECT and, as a consequence, normative data are also becoming available [38, 39].

20 iter   40 iter   60 iter
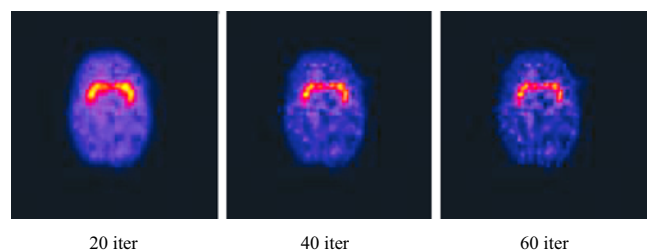
Fig. 3 EM reconstruction of the 6.11:1 filled phantom using 20, 40 and 60 iterations

Table 2 Conventional and LS-ROI estimates of the striatum-to-background ratios in the phantom study

	Acq 1		Acq 2	
	Left	Right	Left	Right
True	6.11	6.11	27.87	9.15
EM-SPECT	3.58	3.42	16.97	5.26
LS-ROI	6.70±0.69	5.77±0.61	27.27±2.59	9.00±0.85

Absolute activity quantification with SPECT is hampered by several factors, such as attenuation, scatter and PVE [40, 41]. Among these effects, the geometrical response of the tomographic system is one of the most important [5, 42]. This effect can be compensated for by means of iterative reconstruction algorithms which include in the reconstruction kernel the geometrical response model [32, 33].

Our results with EM-SPECT reconstruction are one example of this approach. In the absence of noise, such algorithms would give a perfect image restoration, provided the system response is correctly and properly modelled and the number of iterations is adequate. However, the spatial response effect mainly affects the high-frequency components of the image and, consequently, the compensation of spatial resolution is very sensitive to noise. Indeed, our results in the phantom study demonstrate that, in the presence of noise and in spite of a thorough compensation for system spatially variable response, quantification with the EM-SPECT method is less than effective, with a mean underestimation of 42%. In other words, when the algorithm reconstructs individual pixels with a high spatial sampling, SPECT activity quantification is affected by errors even with an advanced reconstruction approach in which the spatial response of the SPECT system is compensated.

The determination of the contents of a few "generalised" pixels is a different task by comparison with the determination of thousands of pixels: the high frequencies implied by the high spatial sampling of the images are not required

in the ROI evaluation problem and propagation of noise on ROI values is less critical. Moreover, in the ROI formulation of the tomographic problem, we have introduced reasonable a priori information about the object, since we have stated that the activity is constant over the ROIs. This information actually changes the original problem (Eq. 4 in the Appendix) into a new one (Eq. 8) which is stable if the number of ROIs is low. Thus, in typical terms of the "inverse problems" jargon, the use of ROIs is a "regularisation technique" and, as a consequence, the LS-ROI method shows improved performance, since it deals with a new problem which is less "ill-conditioned" with respect to the original one.

A similar phantom study was reported by Meyer et al. [43], in which data were acquired with both the triple-head camera MultiSPECT 3 (Siemens Medical Systems, Inc., Hoffman Estates, IL, USA) and the dedicated brain SPECT system Ceraspect (Digital Scintigraphics, Waltham, MA, USA) and reconstructed with filtered back projection (FBP). In that study, an underestimate similar to that in our results was found when the ratios were obtained from images acquired with the triple-head system. On the other hand, ratios estimated from images acquired with the dedicated system were better recovered. Those results can be explained in terms of "ill-conditioning" as well, taking into account that the sensitivity of a dedicated scanner may be 60% higher [43] than that of a triple-head system. Thus, with dedicated systems, the effects of noise are mitigated and the ill-conditioning of the reconstruction problem is reduced.

Table 3 Ratios $R=(C_{st}-C_{cer})/C_{cer}$ obtained in the patient studies with conventional EM-SPECT and LS-ROI methods. Striatal and cerebellar segmented volumes are also shown

Pat. no.	ROI vol. (ml)			EM-SPECT		LS-ROI	
	Left	Right	Cereb	Left	Right	Left	Right
1	7.74	7.27	27.2	5.41	5.17	10.36±1.83	9.73±1.93
2	8.32	8.07	28.2	4.07	3.95	8.10±1.67	8.26±1.50
3	5.78	5.27	32.1	4.03	3.03	6.84±1.09	6.42±1.00
4	5.97	5.36	28.2	6.91	6.82	11.99±2.42	11.47±2.73
5	5.80	5.18	28.2	5.59	5.58	7.72±1.15	7.99±1.07
6	6.40	5.80	29.8	3.36	2.38	4.81±1.30	3.06±1.37
7	6.95	6.46	29.9	1.73	2.00	3.16±1.08	3.59±1.08
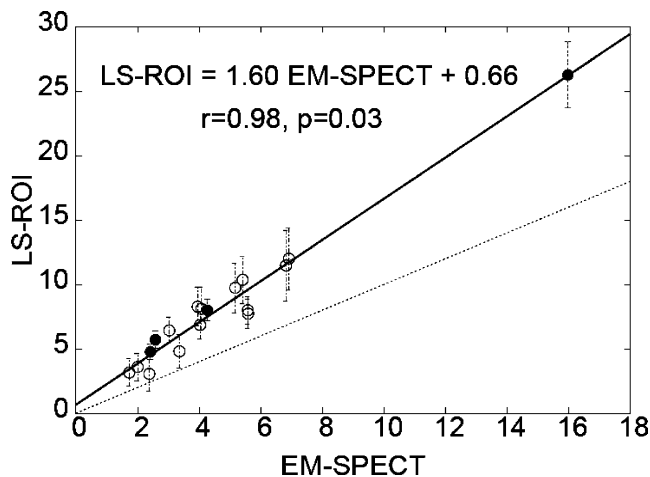
Fig. 4 Correlation between LS-ROI and EM-SPECT estimates: 14 points have been obtained from patient data (*white circles*) and four points from the phantom studies (*black circles*). The regression line is shown in the figure (*continuous line*); the *dashed line* represents identity

Patient studies

In the patients, as in the phantom study, image-based EM-SPECT estimates of BP were lower than the LS-ROI estimates. The linear correlation between the two estimates (Fig. 4) suggests a systematic effect where differences in ratio values measured with the LS-ROI method (ΔLS-ROI) turn to be compressed by a factor 0.625 when measured with EM-SPECT (ΔEM-SPECT): ΔEM-SPECT= 0.625 ΔLS-ROI. Indeed the R range 0–26 obtained with the LS-ROI is reduced to 0–16 with the image-based EM-SPECT method.

A first point to emerge from our results is that the values estimated at 3 h with EM-SPECT are higher than those that can be found in the literature for BP in normal controls. In fact, Tsuchida et al. report [39] a mean BP value of 3.7 ± 0.5 in ten normal controls, both with a single outcome measure at 3 h post injection and with a multilinear regression technique applied to data acquired up to 6 h post injection. Even lower BP values were reported for normal cases in other studies [2, 38, 44]. In all the references cited above, no PVE correction was applied. Our higher estimates in patients and with EM images perhaps can be explained by the fact that the results reported in the literature have often been obtained with images reconstructed by the FBP algorithm and without a geometrical model of the system PSF and, therefore, with lower recovery capabilities. Additionally, it is worth noting that normative data are also camera dependent [10, 43].

A second point to consider is that BP estimates found with the LS-ROI method are even higher than those found with EM-SPECT. If we take into account that an underestimation of up to 50% can be expected when the BP value is measured with images without PVE correction [5], the

LS-ROI estimates in patients may be realistic. Accordingly, in [43], normal subjects acquired with the brain dedicated system indeed gave BP values of around 9.

BP has also been measured with ^{18}F-labelled FP-CIT and PET [12]. In this reference, the acquisition of data ended at 90 min post injection, when the BP with graphical analysis was approximately 3.5. The BP value at 3 h was not measured, but it is not feasible that values as high as ours could have been obtained at that time. A possible reason is that PET measurement, too, was not corrected for PVE.

An interesting comparison can be done with the results in [24], where the same tracer and SPECT system as in our study were used. In [24], the effects of PVE correction were studied in Alzheimer's disease (AD) and dementia with Lewy bodies (DLB). In AD patients, striata can be thought unaffected. For these patients, the PVE correction increased the putamen BP value from 2.9 ± 0.4 to 8.6 ± 1.5.

Limitations of the study

As far as the phantom study is concerned, the choice of Chang's attenuation correction method (with separate contours for each slice) instead of a variable attenuation mask derived from the CT image was motivated by the fact that, in patient studies, CT scans are not always available in a routine context. For instance, CT images were not available for the seven patients analysed in this study, and we wanted to perform the same analysis on both phantom and patient data. Obviously, when an anatomical image is available, the more accurate CT-derived variable attenuation map should be used. In this regard, the increasing diffusion of SPECT/CT systems will help in obtaining more accurate results. However, the use of Chang's correction, a method widely available on commercial SPECT systems, makes our results easy to reproduce and apply in clinical everyday practice.

As far as the patient analysis is concerned, even if our study yielded interesting results, a more accurate study should be performed using CT or MR images for ROI segmentation and accurate definition of the attenuation mask. In the present study both the region segmentation and the (homogeneous) attenuation map definition were based on SPECT images and were therefore prone to errors due to the limited spatial resolution.

PVE correction

Let us now make some comments on PVE correction methods that have to be implemented when image reconstruction is used for quantitative purposes. One of the most popular methods has been proposed by Rousset et al. for PET [13]. In this approach, the mean concentration value c_α ($\alpha=1, ..,N_R$) measured on the images in each of the

ROIs is expressed as a weighted sum of the true activity concentrations in each of the functionally distinct tissue components, C_β ($\beta=1, ..,N_R$):

$$c_\alpha = \sum_{\beta=1}^{N_R} \omega_{\alpha\beta} C_\beta \qquad (1)$$

where the weighting factors $\omega_{\alpha\beta}$ are evaluated starting from the PSF of the PET system. This linear system can be rewritten in matrix form as:

$$c = \Omega C \qquad (2)$$

where the square $N_R \times N_R$ matrix Ω is called the geometric transfer matrix (GTM) and the $N_R \times 1$ vectors c and C are, respectively, the vectors of measured and true concentrations in the ROIs. Equation 2 can be immediately solved for C by matrix inversion.

As we can immediately understand, writing Eq. 1 consists in switching from the ill-conditioned image-reconstruction problem, which has already been solved, to the corresponding ROI problem. In other words, even in Rousset's approach, PVE correction is not due to the (re-) introduction of the geometrical model through the definition of the GTM, as the information about the system response has already been completely used in the image reconstruction step. The activity recovery is due to the introduction of an ROI model for the activity distribution. In comparison with that, with the LS-ROI method, by starting directly with a formulation of the problem in terms of ROIs, we can avoid a second correction step. This explains what we mean by inherent compensation for the PVE in the LS-ROI method.

In order to further compare our approach with the one proposed by Rousset, Eq. 9 in the Appendix can be rewritten in this way:

$$G^T p = (G^T G) X. \qquad (3)$$

Equation 3 can be directly compared with Eq. 2. The true ROI contents are given by vector X and can be estimated from the backprojected image $G^T p$ once the GTM ($G^T G$) has been computed starting from the sinograms that contain all the geometric information.

A difference between the two methods is in the way the GTM is used: in the original approach suggested by Rousset, the GTM relates two "objects", c and C, while in the LS-ROI approach we relate an "object" X, to "projections" p. Therefore, in the LS-ROI method, we just need to model the system PSF in the projection space, while in Rousset approach, the spreading of information has to be described in the object space. The spatial resolution in the object space can be accurately described as a consequence of the geometrical system response in the projection space, in which actually the physical step of radiation detection takes place. In this case, the PSF defined in the projection space is used to project the ROIs and then the GTM is evaluated by reconstructing the ROI sinograms with the same parameters as those used for SPECT or PET data. Otherwise, especially for PET, where modelling the PSF in the projection space is even more complex than for SPECT, the GTM can be evaluated by convolution of the region support with some simplified version of an experimentally measured spatially-variant resolution in the object space. A comparison of these two approaches can be found in [21].

It is also worth to point out that only a PSF model in the projection space allows to directly estimate the regional activity without image reconstruction. This basic feature of the LS-ROI algorithm is a step forward to optimal integration of structural imaging (CT) in molecular imaging (PET/SPECT) as currently offered by hybrid tomographic systems (PET/SPECT-CT).

Conclusion

In this paper, by means of a phantom study, we have demonstrated that the LS-ROI method yields more accurate estimates of tracer concentration in the ROIs than are obtained with the conventional method of summing the content of the pixels of the reconstructed images. The improvement in the accuracy derives from (1) the inclusion of the geometrical system response in the algorithm and (2) the reduced number of unknowns. This approach decreases the ill-conditioning of the problem and allows better compensation for the PVE, once the system response and the statistics are known.

Our phantom study showed that the bias resulting from the conventional method of measuring BP involves a substantial underestimation. The better performance of LS-ROI in the "anthropomorphic" phantom study suggests that the LS-ROI estimates are probably more accurate than the EM-SPECT estimates also in the patients, in whom the true activity concentration is unknown, with the consequence that it is impossible to express a "technical" preference for either of the two reconstruction methods applied.

In patients, EM-SPECT BP values are about 60% of the LS-ROI BP estimates. The measured ranges of BP values are 2-7 and 3-12 with EM-SPECT and LS-ROI, respectively. In other words, a range of 5 BP units, measured with EM-SPECT, becomes a range of 9 BP units with the LS-ROI method. This suggests that the difference between an abnormal and a normal BP could be greater when measured with LS-ROI than when measured with EM-SPECT. This

expansion of diagnostic sensitivity could be strategic in view of the use of DAT SPECT in early PD cases and in "at-risk" subjects as well.

The potential of the LS-ROI method in discriminating between normal control and PD patients has not been assessed thoroughly in this work. The application of the method to a larger group of normal controls and PD patients will constitute the subject of future work. However, these promising results suggest that, from the clinical standpoint, use of the LS-ROI method in BP measurements might enhance the role of receptor molecular imaging in clinical practice.

Appendix

In the LS-ROI method, the generalised inverse is considered for the determination of a set of ROI values from raw tomographic data. The generalised inverse gives the least squares solution to a linear system of equations.

Actually, the tomographic problem can be described using a system of linear equations:

$$p_{km} = \sum_{ij} F_{ij}^{km} Y_{ij} \tag{4}$$

where p_{km} is the measured projection at the m-th angle ($m=1, .., M$), bin k ($k=1,.., K$); Y_{ij} is the number of emitted photons in the object pixel (i, j) and the elements F_{ij}^{km} describe the acquisition process as well as the geometrical system response (resolution, attenuation and scatter). By using a matrix notation, if we call Y the [$IJ{\times}1$] object voxel concentration vector, p the [$KM{\times}1$] projection data set and, finally, F the [$KM{\times}IJ$] projection matrix, the previous equation can be rewritten as:

$$FY = p. \tag{5}$$

Least squares methods seek the minimisation of the functional

$$\chi^2(Y) = \sum_{km} \left(\sum_{ij} F_{ij}^{km} Y_{ij} - p_{km} \right)^2 \Big/ \sigma_{km,}^2 \tag{6}$$

where σ_{km} is the uncertainty with which p_{km} is measured. The solution is given by:

$$Y = \left(F^T \Phi_p^{-1} F \right)^{-1} F^T \Phi_p^{-1} p, \tag{7}$$

where Φ_p^{-1} is the inverse of the projection covariance matrix. Φ_p is a diagonal matrix whose diagonal elements are the variances of the projection data or, if an unweighted fit is performed, $\Phi_p{=}I$.

Equation 7 gives the standard least squares solution to Eq. 4. Application of Eq. 7 to the reconstruction of the tomographic images would be appealing because the solution could be obtained directly, without any iterative procedure, allowing the incorporation of a model of non-stationary factors. Unfortunately, Eq. 7 is extremely ill-conditioned, thus threatening the chance of finding an acceptable physical solution.

Let us suppose that our image space can be divided into a small number N_R of ROIs with constant content, such that $Y_{ij}{=}X^{\alpha}$ for all pixels (i, j) belonging to the region α (R_{α}), where $\alpha=1, ..,N_R$. Equation 4, therefore, becomes:

$$p_{km} = \sum_{\alpha=1}^{N_R} \left(\sum_{(i,j) \in R_{\alpha}} F_{ij}^{km} Y_{ij} \right) = \sum_{\alpha=1}^{N_R} X^{\alpha} \sum_{(i,j) \in R_{\alpha}} F_{ij}^{km}$$
$$= \sum_{\alpha=1}^{N_R} G_{\alpha}^{km} X^{\alpha} \tag{8}$$

where G_{α}^{km} are called "sinograms" of the regions and represent the projection along the ray at bin k, angle m, of an object which is equal to 1 for voxels belonging to region α and 0 elsewhere.

If we call X the [$N_R{\times}1$] region concentration vector and G the [$KM{\times}N_R$] region projection matrix, the (unweighted) least squares solution of Eq. 8 is:

$$X = \left[G^T G \right]^{-1} G^T p. \tag{9}$$

Since we have introduced a lot of a priori information about the solution (which is constant over the ROIs), the ill-conditioning of the "ROI" problem (Eq. 9) is strongly reduced with respect to the original "voxel" problem (Eq. 7). Therefore, the solution can be computed directly from projections by using Eq. 9, once regions have been segmented in some way and the sinograms G_{α}^{km} for each region have been obtained from the weighting factors F_{ij}^{km}. Therefore, region activity evaluation is not performed with reconstructed images.

The covariance matrix of the solution can also be computed and is given by:

$$\Phi_x = \left[G^T G \right]^{-1} G^T \Phi_p G \left[G^T G \right]^{-1}. \tag{10}$$

References

1. Innis RB, Seybil JB, Scanley BE, Laruelle M, Abi-Dargham A, Wallace E, et al. Single photon computed tomographic imaging demonstrates loss of striatal dopamine transporters in Parkinson disease. Proc Natl Acad Sci U S A 1993;90(24):11965–69.

2. Booij J, Habraken JB, Bergmans P, Tissingh G, Winogrodzka A, Wolters EC, et al. Imaging of dopamine transporters with iodine-123-FP-CIT SPECT in healthy controls and patients with Parkinson's disease. J Nucl Med 1998;39(11):1879–84.

3. Mozley PD, Schneider JS, Acton PD, Plossl K, Stern MB, Siderowf A, et al. Binding of [^{99m}Tc]TRODAT-1 to dopamine transporters in patients with Parkinson's disease and in healthy volunteers. J Nucl Med 2000;41(4):584–9.

4. Acton PD, Newberg A, Plossl K, Mozley PD. Comparison of region-of-interest analysis and human observers in the diagnosis of Parkinson's disease using [^{99m}Tc]TRODAT-1 and SPECT. Phys Med Biol 2006;51(3):575–85.

5. Soret M, Koulibaly PM, Darcourt J, Hapdey S, Buvat I. Quantitative accuracy of dopaminergic neurotransmission imaging with ^{123}I SPECT. J Nucl Med 2003;44(7):1184–93.

6. Hashimoto J, Sasaki T, Ogawa K, Kubo A, Motomura N, Ichihara T, et al. Effects of scatter and attenuation correction on quantitative analysis of β-CIT brain SPET. Nucl Med Commun 1999;20(2):159–65.

7. Kojima A, Matsumoto M, Takahashi M, Hirota Y, Yashida H. Effect of spatial resolution on SPECT quantification values. J Nucl Med 1989;30(4):508–14.

8. Clarke LP, Leong LL, Serafini AN, Tyson IB, Silbiger ML. Quantitative SPECT imaging: influence of object size. Nucl Med Commun 1986;7(5):363–72.

9. Jaszczak JR, Coleman RE, Withehead FR. Physical factors affecting quantitative measurement using camera based single photon emission computed tomography (SPECT). IEEE Trans Nucl Sci 1981;28:69–80.

10. Koch W, Radau PE, Munzing W, Tatsch K. Cross-camera comparison of SPECT measurements of a 3-D antropomorphic basal ganglia phantom. Eur J Nucl Med Mol Imag 2006;33(4):495–502.

11. Chaly T, Dhawan V, Kazumata K, Antonini A, Margouleff C, Dahl JR, et al. Radiosynthesis of [^{18}F]N-3-fluoropropyl-2β-carbomethoxy-3-β-(4-iodophenyl) nortropane and the first human study with positron emission tomography. Nucl Med Biol 1996;23:999–1004.

12. Kazumata K, Dhawan V, Chaly T, Antonini A, Margouleff C, Belakhlef A, et al. Dopamine transporter imaging with fluorine-18-FPCIT and PET. J Nucl Med 1998;39(9):1521–30.

13. Rousset OG, Ma Y, Evans AC. Correction for partial volume effects in PET: principle and validation. J Nucl Med 1998;39(5):904–11.

14. Cooke BE, Evans AC. A phantom to assess quantitative recovery of positron tomographs. J Comput Assist Tomogr 1983;7(5):876–80.

15. Mullani NA. A phantom for quantitation of partial volume effects in ECT. IEEE Trans Nucl Sci 1989;36(1):983–7.

16. Hoffman EJ, Huang SC, Phelps ME. Quantitation in positron emission computed tomography: 1. Effect of object size. J Comput Assist Tomogr 1979;3(3):299–308.

17. Mahoney DK, Huang SC, Ricci AR, Mazziotta JC, Hoffman EJ, Phelps ME. A realistic computer simulated brain phantom for evaluation of PET characteristics. IEEE Trans Med Imag 1987;6:250–7.

18. Meltzer CC, Leal JP, Mayberg HS, Wagner HN, Frost JJ. Correction of PET data for partial volume effects in human cerebral cortex by MR imaging. J Comput Assist Tomogr 1990;14(4):561–70.

19. Muller-Gartner HW, Links JM, Prince JL, Bryan RN, McVeigh E, Leal JP, et al. Measurement of radiotracer concentration in brain gray matter using positron emission tomography: MRI-based correction for partial volume effects. J Cereb Blood Flow Metab 1992;12(4):571–83.

20. Meltzer CC, Zubieta JK, Links JM, Brakeman P, Stumpf MJ, Frost JJ. MR-based correction of brain PET measurements for heterogeneous gray matter radioactivity distribution. J Cereb Blood Flow Metab 1996;16(4):650–8.

21. Frouin V, Comtat C, Reilhac A, Gregoire MC. Correction for partial volume effect for PET striatal imaging: fast implementation and study of robustness. J Nucl Med 2002;43(12):1715–26.

22. Quarantelli M, Berkouk K, Prinster A, Landeau B, Svarer C, Balkay L, et al. Integrated software for the analysis of brain PET/SPECT studies with partial-volume-effect correction. J Nucl Med 2004;45(2):192–201.

23. Du Y, Tsui BMW, Frey EC. Partial volume effect compensation for quantitative brain SPECT imaging. IEEE Trans Med Imag 2005;24(8):969–76.

24. Soret M, Koulibaly PM, Darcourt J, Buvat I. Partial volume effect correction in SPECT for striatal uptake measurements in patients with neurodegenerative diseases: impact upon patient classification. Eur J Nucl Med Mol Imag 2006;33(9):1062–72.

25. Formiconi AR. Least squares algorithm for region of interest evaluation in emission tomography. IEEE Trans Med Imag 1993;12(1):90–100.

26. Vanzi E, Formiconi AR, Bindi D, La Cava G, Pupi A. Kinetic parameter estimation from renal measurements with a three-headed SPECT system: a simulation study. IEEE Trans Med Imag 2004;23(3):363–73.

27. Huesman RH. A new fast algorithm for the evaluation of regions of interest and statistical uncertainty in computed tomography. Phys Med Biol 1984;29(5):543–52.

28. Muzic RF, Chen CH, Nelson AD. A method to correct for scatter, spillover, and partial volume effects in region of interest analysis in PET. IEEE Trans Med Imag 1998;17(2):202–13.

29. Chen CH, Muzic RF, Nelson AD, Adler LP. Simultaneous recovery of size and radioactivity concentration of small spheroids with PET data. J Nucl Med 1999;40(1):118–30.

30. Carson RE. A maximum likelihood method for region-of-interest evaluation in emission tomography. J Comput Assist Tomograph 1986;10(4):654–63.

31. Da Silva AJ, Tang HR, Wong KH, Wu MC, Dae MW, Hasegawa BH. Absolute quantification of regional myocardial uptake of ^{99m}Tc-sestamibi with SPECT: experimental validation in a porcine model. J Nucl Med 2001;42(5):772–9.

32. Formiconi AR, Passeri A, Calvini P. Theoretical determination of the collimator geometrical transfer function for the reconstruction of SPECT data. IEEE Trans Nucl Sci 1999;46(4):1075–80.

33. Boccacci P, Bonetto P, Calvini P, Formiconi AR. A simple model for the efficient correction of collimator blur in 3D SPECT imaging. Inverse Problems 1999;15:907–30.

34. Minoshima S, Koeppe RA, Frey KA, Kuhl D. Anatomic standardization: linear scaling and nonlinear warping of functional brain images. J Nucl Med 1994;35(9):1528–37.

35. Rorden C, Brett M. Stereotaxic display of brain lesions. Behav Neurol 2000;12(4):191–200.

36. Gelb D, Oliver E, Gilman S. Diagnostic criteria for Parkinson disease. Arch Neurol 1999;56(1):33–9.

37. Bertero M, Boccacci P. Introduction to inverse problems in imaging. Bristol and Philadelphia: Institute of Physics Publishing; 1998.

38. Lavalaye J, Booij J, Reneman L, Habraken JB, van Royen EA. Effect of age and gender on dopamine transporter imaging with [^{123}I]FP-CIT SPET in healthy volunteers. Eur J Nucl Med Mol Imag 2000;27(7):867–9.

39. Tsuchida T, Ballinger JR, Vines D, Kim YJ, Utsunomiya K, Lang AE, et al. Reproducibility of dopamine transporter density measured with ^{123}I-FPCIT SPECT in normal control and Parkinson's disease patients. Ann Nucl Med 2004;18(7):609–16.

40. Du Y, Tsui BMW, Frey EC. Model-based compensation for quantitative ^{123}I brain SPECT imaging. Phys Med Biol 2006;51(5):1269–82.

41. Kim KM, Varrone A, Watabe H, Shidahara M, Fujita M, Innis RB, et al. Contribution of scatter and attenuation compensation to SPECT images of nonuniformly distributed brain activities. J Nucl Med 2003;44(4):512–9.

42. Cot A, Falcon C, Crespo C, Sempau J, Pareto D, Bullich S, et al. Absolute quantification in dopaminergic neurotransmission SPECT using a Monte Carlo-based scatter correction and fully 3-dimensional reconstruction. J Nucl Med 2005;46(9):1497–504.

43. Meyer PT, Sattler B, Lincke T, Seese A, Sabri O. Investigating dopaminergic neurotransmission with ^{123}I-FP-CIT SPECT: comparability of modern SPECT systems. J Nucl Med 2003;44(5):839–45.

44. Lorberboym M, Djaldetti R, Melamed E, Sadeh M, Lampl Y. ^{123}I-FP-CIT SPECT imaging of dopamine transporters in patients with cerebrovascular disease and clinical diagnosis of vascular parkinsonism. J Nucl Med 2004;45(10):1688–93.